THE JOURNAL OF PHYSICAL CHEMISTRY B

Article

pubs.acs.org/JPCB

Comparison of the Thermal Denaturing of Human Serum Albumin in the Presence of Guanidine Hydrochloride and 1-Butyl-3-methylimidazolium Ionic Liquids

William T. Heller*

Biology and Soft Matter Division, Oak Ridge National Laboratory, Oak Ridge, Tennessee 37831, United States

Supporting Information

ABSTRACT: The interaction of proteins with aqueous solutions of ionic liquids (ILs) has attracted considerable recent attention owing to the challenges of finding biocompatible water-free ILs. These systems remain of great interest because of the potential for using ILs as designer solvents for biocatalytic processes. Increasing evidence demonstrates that aqueous solutions of water-miscible ILs, such as the well-studied 1-alkyl-3-methylimidazolium ILs, disrupt the native fold of proteins and can drive the formation of non-native aggregates that could negatively impact catalytic function. Here, we present a study comparing the thermal unfolding of human serum albumin (HSA) in a 1 M solution of the protein denaturant guanidine hydrochloride with two 1 M aqueous solutions of 1-butyl-3-methylimidazolium ILs, namely the chloride and the acetate. Small-angle neutron scattering (SANS) measurements found qualitative agreement between the thermally driven unfolding process for the three denaturants, as well as with a Tris buffer solution. HSA irreversibly aggregates and unfolds in the three denaturant solutions upon heating to temperatures below that required to drive the same process in a simple Tris buffer solution. The results reveal subtle differences in the interaction of the ILs and guanidine hydrochloride with the protein, although the final states of the protein were similar in all cases. The results indicate that the ions of water-miscible ILs and guanidine hydrochloride have specific roles in disrupting protein structure and driving aggregation. The experimental approach employed has the potential to provide new insights into protein interactions with ionic liquids that may aid in the search for more biocompatible ionic liquids.

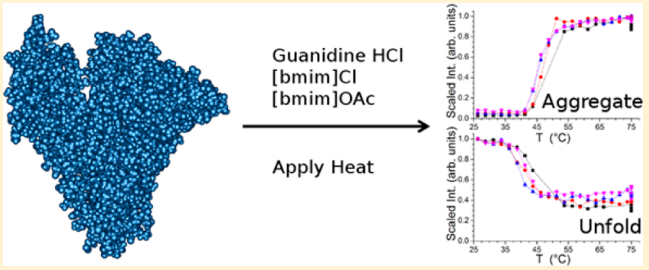

The use of ionic liquids (ILs), salts that are molten at temperatures below 100 °C, as solvents for chemical processes continues to attract a great deal of attention.[1−4] The vast diversity of chemical and physical properties of ILs enables tuning of solvent conditions for improved and selective solubility of reactants and products. Further, the recyclability and negligible vapor pressure compared to organic solvents make ILs attractive for "green chemistry" applications.[5] Unlike other chemical reactions, the development of ionic liquids for biocatlytic applications has been slower but continues to progress.[6−10] The main challenge lies in finding a suitable IL that dissolves a protein in a functional state at sufficient loading without water. The nearly infinite variability of the physical and chemical properties of the surfaces of proteins makes finding a universally applicable, dry IL for biocatalytic applications a daunting task.

Although the search for more biocompatible, dry ILs continues, a great deal of recent work has focused on protein structure and function in water/IL mixtures. Such solvents represent a compromise in which the water serves to improve the solubility of the proteins, whereas the IL lends some amount of its physicochemical properties to the solvent. Two approaches exist that depend on the water-miscibility of the IL being used. Water-immiscible ILs are suited for forming water-in-IL microemulsions that provide an aqueous environment thought to improve protein solubility and activity surrounded by the IL. Such systems have been demonstrated for biocatalytic applications employing lipases,[11,12] horseradish peroxidase,[13] lignin peroxidase,[14] and laccase.[14,15] The microemulsions are stabilized by surfactants, such as AOT (sodium bis(2-ethyl-1-hexyl)sulfosuccinate),[11−13] Triton X-100,[12,14] or both surfactants,[15] which provides an interface between the IL and aqueous phases. In some cases, 1-hexanol[11] and isooctane[13] cosurfactants were also employed.

In contrast, aqueous solutions of water-miscible ILs have become more common as solvents for biocatlysis, resulting in several studies of protein structure and function. Extensive characterization of enzymes in aqueous IL solutions by Zhao and co-workers produced a Hofmeister series ranking the protein stabilizing properties of various cations and anions, which provides a valuable tool for selecting suitable ILs for biocatalytic applications.[16,17] The activity of an *A. niger* cellulase decreased to 40% of its native value in solutions up to 25 vol.% [bmim]Cl,[18] and a similar decrease in activity was observed for

Received: January 3, 2013
Revised: February 5, 2013
Published: February 6, 2013

horseradish peroxidase in aqueous solutions of other water-miscible ILs.[19] Studies of cytochrome c in biocompatible ILs, such as [bmim] or choline paired with dihydrogen phosphate, containing 20 vol % water allowed for long-term storage and dissolved the protein at concentrations up to 3 mM.[20−22] Serum albumins, whether human or bovine, have been shown to denature in aqueous solutions of many different ILs,[23−28] as does green fluorescent protein.[29] The variety of properties of ILs available affords a broad spectrum of responses in protein structure and function.

To improve the understanding of the specific consequences of protein−IL interactions and begin to tease out the mechanisms involved, detailed biophysical studies are required. In the present study, the temperature-dependent behavior of HSA in aqueous solutions of two [bmim] ionic liquids, namely the chloride and the acetate, were compared to that in a simple buffer solution and in a guanidine hydrochloride solution, a commonly used protein denaturant. The structure and aggregation state of the protein in response to elevated temperatures was monitored using small-angle neutron scattering (SANS), a nondestructive method that can probe the solution structure and aggregation state of proteins.[30] The application of small-angle scattering methods, whether X-ray or neutron, to the study of biological macromolecules in solution has been described in detailed reviews.[31−33] The protein responds to heating in the four solvents by both unfolding and aggregating in a similar manner, but subtle differences in the temperature-dependent behavior do exist. The relative sensitization of HSA to thermal denaturation caused by GdnHCl and the ILs are made clear by the SANS data and make it possible to understand the role of the cations and anions in the denaturing processes occurring at different length scales. The methodology employed here can be used to better understand ion-specific protein-IL interactions, and could prove of use in understanding the impact of other salts on protein stability in solution.

MATERIALS AND METHODS

Sample Preparation. Essentially fatty acid-free HSA was obtained from Sigma-Aldrich (product A3782; St. Louis, MO, USA) as a lyophilized powder. 1-Butyl-3-methylimidazolium chloride (product 94128) and 1-butyl-3-methylimidazolium acetate (product 39952) were obtained from Aldrich (St. Louis, MO, USA). Tris HCl (product 04816100), Tris base (product TRIS01KG), and guanidine hydrochloride (product 11GUAC500G) were obtained from MP Biomedicals, Inc. (Solon, OH, USA). All materials were used without further purification. Stock solvents (20 mM Tris, pH 7.4; 1 M GdnHCl, 1 M [bmim]Cl, and 1 M [bmim]OAc) were made with D_2O (99.8% isotopic D; product DLM-4-99.8-1000; Cambridge Isotope Laboratories; Cambridge, MA, USA). The use of D_2O maximized the scattering length density contrast between the protein and solvent in all cases while minimizing the incoherent scattering from hydrogen in the samples. Protein solutions for the SANS experiments were made at 10 mg/mL in the stock solvents by dissolving the protein powder in the appropriate amount of solution. All samples were passed through a 0.22 μm syringe filter to remove any high molecular weight contaminants and aggregates. Samples were stored at 5 °C prior to the start of the SANS measurements, which began within 72 h of preparing the solutions.

SANS Measurements. SANS data were collected using the EQ-SANS instrument of the Spallation Neutron Source of Oak Ridge National Laboratory.[34] The sample-to-detector distance was set to 4.0 m. A 25 mm source aperture and a 10 mm sample aperture were used to collimate the incident beam. The instrument was operated in the 30 Hz "frame-skipping" mode with a minimum wavelength setting of 2.5 Å, providing a second wavelength band starting at 9.4 Å and affording a combined q-range ($q = 4\pi \sin(\theta)/\lambda$; 2θ is the scattering angle and λ is the wavelength) that covered 0.007−0.40 Å^{-1} to allow for data reduction and analysis. The momentum transfer of the neutron, q, is related to the distance being probed, d, through the relation $q = 2\pi/d$. The useful q-range provided by the instrument configuration employed was 0.007−0.25 Å^{-1}. Data correction followed standard procedures implemented in MantidPlot (http://www.mantidproject.org/) to correct for sample transmission, detector sensitivity, and dark current before azimuthally averaging the 2D data to produce $I(q)$ vs q. The data from the two wavelength bands were merged into a single profile using MantidPlot. The data were then corrected for the protein-free solution scattering to provide the final, reduced SANS intensity profiles.

Two different temperature series were collected on the four samples. In each case, a single aliquot of the sample was measured at all temperature settings. Neutrons are non-destructive, so the samples did not degrade from radiation damage during exposure. In the first temperature series, data were collected at a set of equilibrated temperatures ranging from 20 to 65 °C, as controlled by a water bath using the EQ-SANS standard sample changer.[34] A final data set for each sample was collected after returning the temperature to 20 °C. In the second type of measurement performed, a furnace employing cartridge heaters was used that allowed for accurate control of the temperature ramp rate. The temperature for each sample, mounted in the furnace individually, was ramped from 25 to 75 °C at 0.5 °C/min. Data on EQ-SANS are natively collected in "event mode" where the series of neutron detector coordinates and arrival times are stored for later processing. The data reduction software was used to parse the continuous stream of data collected during the measurement into time bins to track the behavior of the system during the temperature ramp.

SANS Data Analysis. Small-angle scattering methods, whether or X-rays or neutrons, can be applied to a vast array of materials to obtain structural information ranging from sizes and shapes of particles in dilute solution to morphological parameters in complex hierarchical structures.[35] SANS data were analyzed using a variety of strategies. In cases where the signal clearly resulted from a solution of discrete particles, Guinier analysis[36] for the radius of gyration, R_g, was performed. R_g is analogous to the mechanical radius of gyration of an object and is a measure of the compactness of a scattering particle, making it very sensitive to protein denaturation. Such data were also fit for the distance distribution function, $P(r)$, using the implementation of the Moore algorithm[37] in SANSView (http://danse.chem.utk.edu/sansview.html). $P(r)$ is a measure of the frequency of distances between scattering centers (nuclei or electrons) within a scattering particle and provides more information regarding particle shape than R_g does alone. Fitting SANS data from a dilute protein solution for $P(r)$ also provides the maximum linear dimension, D_{max}, of the scattering particle, which is the longest distance between scattering centers in it. SANS data from a solution of discrete particles were also compared to the intensity profile calculated from the monomer extracted from the crystal structure of HSA (PDB ID: 1AO6[38])

dx.doi.org/10.1021/jp400079p | J. Phys. Chem. B 2013, 117, 2378−2383

using ORNL_SAS.[39] In cases where such analysis was not appropriate because the data were not consistent with a solution of discrete particles, the SANS data were modeled as a long, flexible cylinder with a polydisperse radius, as provided in the National Institute of Standards and Technology (NIST) SANS data analysis routines[40] and implemented in IgorPro (Wavemetrics, Inc., Lake Oswego, OR). The SANS intensity at specific q-values was also read from the data as a function of temperature to track qualitative changes in the structure during the measurements.

RESULTS

SANS data collected at the start point (25 °C) and end point (75 °C) of the temperature ramp are shown in Figure 1. The

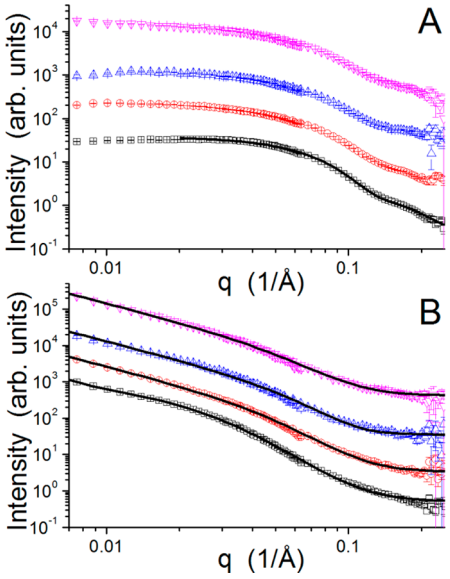

Figure 1. (A) SANS intensity profiles of the HSA solutions at the final temperature (25 °C) in Tris buffer (black), 1 M GdnHCl (red), 1 M [bmim]Cl (blue), and 1 M [bmim]OAc (magenta). The solid black line is the intensity profile calculated from the crystal structure of HSA (PDB ID: 1AO6[38]) using ORNL_SAS.[39] (B) SANS intensity profiles of the HSA solutions at the final temperature (75 °C) in Tris buffer (black), 1 M GdnHCl (red), 1 M [bmim]Cl (blue), and 1 M [bmim]OAc (magenta). The solid black lines are the fits using the flexible cylinder with polydisperse radius model provided in the NIST SANS data analysis suite.[40]

difference in signal-to-noise between the various buffers results from the different scattering length densities of the various solvents. The 1 M GdnHCl and the ILs reduced the contrast between the protein and the solvent, which decreased the signal strength. The use of D_2O in this study greatly improved the signal quality over previous work performed in H_2O.[23] The SANS data collected in the four solutions at the start of the temperature ramp are not the same, indicating differences in the starting HSA structure. The initial SANS data collected in the buffer solution is consistent with the SANS profile calculated from the crystal structure of HSA (PDB ID: 1AO6[38]) using ORNL_SAS[39] (the solid line shown with the data). The $P(r)$ curves produced by fitting the data are presented in Figure 2. The data collected in 1 M GdnHCl and the ILs show very similar protein conformations that are more extended, as evidenced by the larger maximum linear dimension D_{max} (85 Å), than is found in the buffer solution

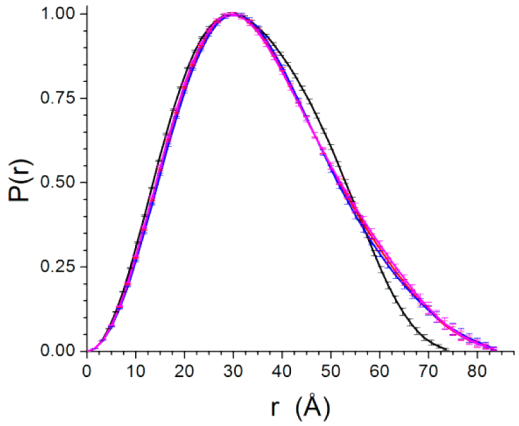

Figure 2. $P(r)$ curves determined from the initial temperature (25 °C) SANS data derived from the initial temperature (25 °C) SANS data for the HSA solutions in Tris buffer (black), 1 M GdnHCl (red), 1 M [bmim]Cl (blue), and 1 M [bmim]OAc (magenta).

(75 Å). The R_g determined from the second moment of $P(r)$, which is not as strongly impacted by the interparticle interference artifacts observable at low-q in some of the data sets, as would be the case for a traditional Guinier fit,[36] are 25.9 ± 0.1 Å (Tris buffer), 27.2 ± 0.1 Å (GdnHCl), 27.3 ± 0.1 Å ([bmim]Cl), and 27.3 ± 0.1 Å ([bmim]OAc). The SANS data collected in GdnHCl and the ILs at 25 °C are not consistent with a highly unfolded HSA[23] or an unfolded state of the related protein bovine serum albumin.[41,42]

The difference between the initial, 25 °C SANS data (Figure 1A) and the data collected at 75 °C after the temperature ramp finished (Figure 1B) is dramatic. The transition between the two states can be seen in the SANS data shown in Figure 3, which are 5 min time slices of the event streams collected for each sample during the temperature ramp. The HSA transitions between monomers to much larger aggregates, based on the dramatic increase in the scattering at low-q. The low-q scattering scales with the square of the molecular weight of the scattering object and linearly with concentration, so the 10-fold increase in the scattering at the lowest q-values would indicate that the aggregates are at least 10 times the molecular weight of the monomer, but the likely mass-fractal character of the aggregates, which are larger than the length scales probed during the measurements, and may be larger than are accessible to the instrument, suggests that the samples have adopted a highly polydisperse character. The fit curves shown in Figure 1B were obtained using the form factor for a long, flexible rod with a polydisperse radius,[40] and the structural parameters from the fit are presented in Table S1, Supporting Information. In all cases, the structure is long and slender (Table S1, Supporting Information), having a radius that is less than the D_{max} of the folded protein.[38] The Kuhn length found by the fitting for the three denaturants was considerably smaller than that found in the Tris buffer, raising the possibility that the unfolding was not as complete in the Tris buffer as in the other solutions. Although the low-q data indicate the growth of large structures, the SANS data show a change in character at high q, which can also be seen in Figure 3, and suggest an unfolding of the polypeptide chain. The unfolding and aggregation were irreversible. Returning the temperature to 20 °C after a measurement at 65 °C, done during the equilibrated temperature series of measurements, did not return the samples to

dx.doi.org/10.1021/jp400079p | J. Phys. Chem. B 2013, 117, 2378−2383

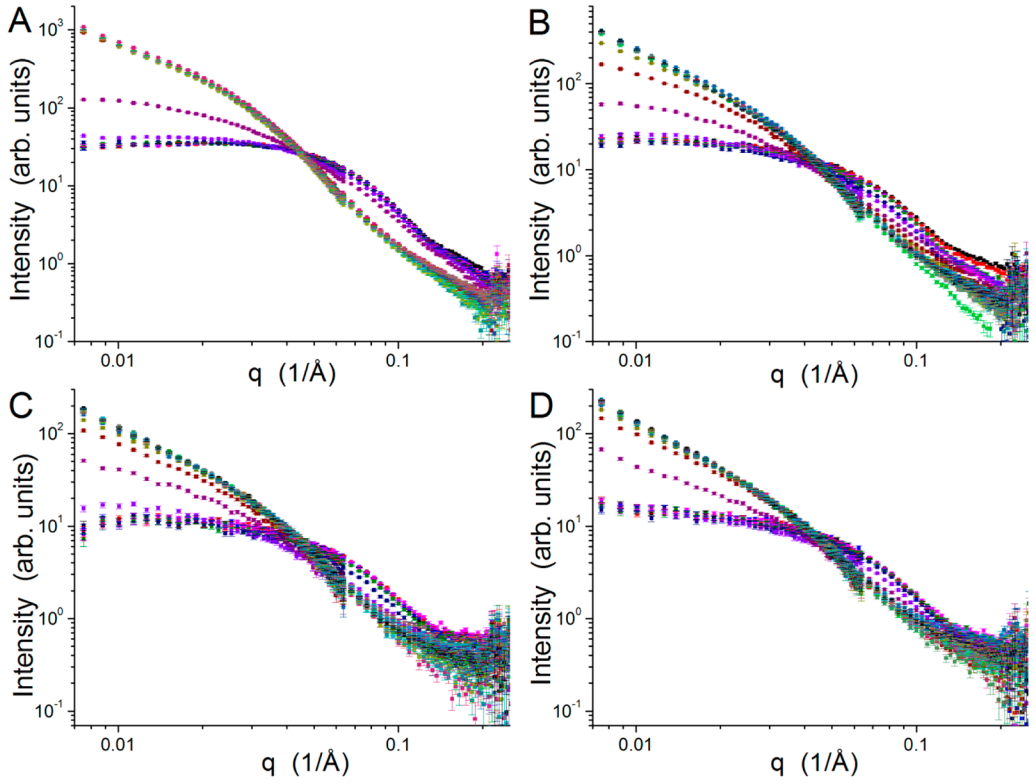

Figure 3. SANS data collected during the 0.5 °C/min temperature ramp measurements parsed every 5 min for HSA solutions in (A) Tris buffer, (B) 1 M GdnHCl, (C) 1 M [bmim]Cl and (D) 1 M [bmim]OAc. There is a gap in the temperature sequence in the SANS data during a 15 min period during the measurement of the sample in Tris buffer when the SNS facility was not producing neutrons.

their initial, monodisperse state (Figure S1, Supporting Information).

The temperature dependence of the transition between the two states is smooth and fairly rapid with temperature, as can be seen in Figure 3. The transition can be more clearly seen in Figure 4 where the intensity relative to the starting value at 25 °C at q = 0.0075 Å^{-1} (Figure 4A) and q = 0.077 Å^{-1} (Figure 4B) are plotted as a function of temperature. Although the lower q-value is representative of length scales relevant to the aggregate growth process, the higher q-value is more representative of those related to the tertiary structure of HSA and can be used to track the fold of the polypeptide chain. Clear differences exist between the HSA structural transition temperatures in the solutions studied. GdnHCl drives the transition at the shorter length scales at a lower temperature than it does in the Tris buffer solution, whereas the transition at longer length scales takes place at nearly the same temperature, although the gap in the Tris buffer data resulting from a loss of beam during the measurement leaves a gap in the temperature series during the transition at these length scales. The measurements of HSA in Tris buffer went for a slightly longer period of time at 75 °C and indicate that the aggregates dissociate to some degree when incubated at this temperature. The data also indicate that the transition to the final aggregation state for HSA in the GdnHCl solution is sharper than in the other solutions. Interestingly, the structural transition of HSA in GdnHCl at the shorter length scales is more gradual with temperature than at the longer length scales, as well as relative to the transition observed for HSA at these length scales in the other solutions. The effect is subtle, and the noise in the data and experimental uncertainty prevents the differences from being unambiguous. Both [bmim]Cl and

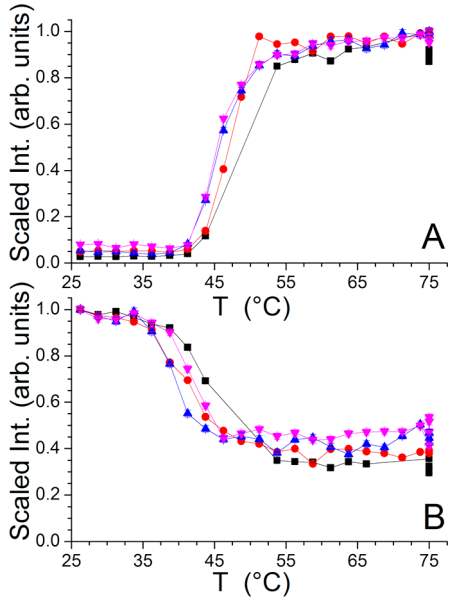

Figure 4. Values of the SANS intensity relative to the intensity value at the starting temperature (25 °C) at q = 0.0075 Å^{-1} (A) and q = 0.077 Å^{-1} (B) as a function of temperature during the temperature ramp measurements for the HSA solutions in Tris buffer (black), 1 M GdnHCl (red), 1 M [bmim]Cl (blue), and 1 M [bmim]OAc (magenta). There is a gap in the temperature sequence in the SANS data during a 15 min period during the measurement of the sample in Tris buffer when the SNS facility was not producing neutrons.

[bmim]OAc cause the aggregation process to begin at a lower temperature than occurs in either Tris buffer or GdnHCl, but

dx.doi.org/10.1021/jp400079p | J. Phys. Chem. B 2013, 117, 2378−2383

the onset of aggregation happens at the same temperature in both ILs. The transition to the final, aggregated state in the ILs is more gradual with temperature than it is in the GdnHCl solution (Figure 4A). In contrast, the changes at the shorter length scales begin at a lower temperature in [bmim]Cl than [bmim]OAc. In this case, the relative onset temperatures are [bmim]Cl ~ GdnHCl < [bmim]OAc ~ Tris.

DISCUSSION

The results presented here demonstrate that the irreversible, thermally driven unfolding and aggregation of HSA by GdnHCl and two [bmim]-based ILs share a common pathway and final structural state of the protein, which is also consistent with the thermal denaturation of the protein in Tris buffer. At an equimolar concentration, GdnHCl and the two ILs sensitize HSA to thermal denaturation relative to the Tris buffer. It has been previously observed that GdnHCl and [bmim]Cl are similarly potent denaturants on an equimolar basis,[43] and the present results support this conclusion. Many ILs, including [bmim]Cl, denature proteins more effectively with increasing concentration,[23−29] much like urea[41] and GdnHCl.[43] For those materials not possessing surfactant-like structures with longer alkyl chains, concentrations above 1 M generally result in significant unfolding without subjecting the protein to elevated temperatures. Interestingly, the differences between the denaturant-driven behavior at the interparticle and intraparticle length scales revealed by the temperature series of SANS data measured in the present study suggest that specific behaviors can be attributed to the cation and anion.

The present results are consistent with a previous study that found OAc^- to be less disruptive of protein structure than Cl^-.[22] The effect obviously cannot be solely attributed to the different anions, because none of the interactions present in solution take place in the absence of the cations. The net effect of the interaction of the various groups with the protein drives the disruption of the protein fold. The similar onset temperature for the changes in the SANS data resulting from the intraparticle distances (Figure 4B) for GdnHCl and [bmim]Cl support the idea that the Cl^- anion is driving the disruption of the HSA fold rather than the aggregation of the protein. It is very interesting to note the differences in the slope of the GdnHCl and [bmim]Cl curves in Figure 4B, as well as the similarity of the slopes of the [bmim]Cl and [bmim]OAc curves in the same figure. This comparison suggests that the anion dictates the temperature of unfolding, but the cation dictates the structural transitions involved in the process. Though a very speculative statement, the effect merits further investigation.

The SANS data also show differences in the interparticle interactions that exist in the solutions. From Figure 4A, one can see that the transition of HSA to the aggregated state in GdnHCl happens more abruptly as a function temperature than it does for either of the ILs studied, which display almost identical behaviors at these length scales. At 10 mg/mL, the protein occupies on the order of 1% of the volume of the solution. At the concentration of denaturants used in this study, all long-range electrostatic interactions are well-screened. Therefore, the data suggest that the changes in the interparticle interactions caused by the three denaturants are the result of association of the $[bmim]^+$ and Gdn^+ with the surface of the protein, creating a more attractive protein−protein interaction in the GdnHCl solution than in the IL solutions. Previous work found that $[bmim]BF_4$ competes with fatty acids for binding sites on the surface of HSA,[24] indicating that such binding could take place without competition from a fatty acid. Although the alkyl chain is very short, $[bmim]^+$ has an amphiphillic structure, whereas the Gdn^+ does not. By shielding the hydrophobic patches normally occupied by a fatty acid, the $[bmim]^+$ may reduce the tendency of the proteins to aggregate. A decrease in the $[bmim]^+$ binding to the patches on HSA at increased temperature could delay the onset of aggregation with temperature, but the eventual exposure of groups shielded by the native fold of the protein eventually overcomes the effect, allowing aggregate growth to take place as shown in Figure 4A.

CONCLUSIONS

SANS was used to characterize the structural transitions that take place during thermal denaturing of the model protein HSA in the presence of GdnHCl and the ILs [bmim]Cl and [bmim]OAc. The results bring to light subtle differences that exist between the interaction of the various ions studied with the protein that manifest across a range of length scales and provide new insight into specific roles that exist for the anions and cations in the disruption of the tertiary structure of the protein and the interactions that lead to its aggregation during heating. The approaches employed here could prove invaluable for investigating other protein-ionic liquid interactions, as well as the Hofmeister effects of other salts.

ASSOCIATED CONTENT

Supporting Information

Structural parameters from the flexible cylinder model fitting of the SANS data collected at 75 °C and representative SANS data from the equilibrated temperature series for the four solvent conditions studied. This material is available free of charge via the Internet at http://pubs.acs.org/.

AUTHOR INFORMATION

Corresponding Author

*Phone: 865-241-0093. Fax: 865-574-6080. E-mail: hellerwt@ornl.gov.

Author Contributions

W.T.H. designed the research, collected and analyzed the data, and wrote the manuscript.

Notes

The authors declare no competing financial interest.

ACKNOWLEDGMENTS

The author thanks Gregory S. Smith for providing thoughtful comments on the manuscript. Research at Oak Ridge National Laboratory's Spallation Neutron Source was sponsored by the Scientific User Facilities Division, Office of Basic Energy Sciences, U.S. Department of Energy. Oak Ridge National Laboratory is managed by UT-Battelle, LLC, for the U.S. Department of Energy under contract No. DE-AC05-00OR22725.

ABBREVIATIONS:

SANS, small-angle neutron scattering; ionic liquid, IL; HSA, human serum albumin; [bmim]Cl, 1-butyl-3-methylimidazolium chloride; [bmim]OAc, 1-butyl-3-methylimidazolium acetate; GdnHCl, guanidine hydrochloride

REFERENCES

(1) Welton, T. Room-Temperature Ionic Liquids. Solvents for Synthesis and Catalysis. *Chem. Rev.* **1999**, *99* (8), 2071−2083.
(2) Gordon, C. M. New Developments in Catalysis using Ionic Liquids. *Appl. Catal. A* **2001**, *222* (1−2), 101−117.
(3) Sheldon, R. Catalytic Reactions in Ionic Liquids. *Chem. Commun.* **2001**, *23*, 2399−2407.
(4) Plechkova, N. V.; Seddon, K. R. Applications of Ionic Liquids in the Chemical Industry. *Chem. Soc. Rev.* **2008**, *37* (1), 123−150.
(5) Horvath, I. T.; Anastas, P. T. Innovations and Green Chemistry. *Chem. Rev.* **2007**, *107* (6), 2169−2173.
(6) Kragl, U.; Eckstein, M.; Kaftzik, N. Enzyme Catalysis in Ionic Liquids. *Curr. Opin. Biotechnol.* **2002**, *13* (6), 565−571.
(7) Liu, Q. B.; Zhang, Z. H.; Zhang, F. J. Progress in Biocatalytic Reactions in Ionic Liquids. *Prog. Chem.* **2005**, *17* (6), 1060−1066.
(8) Xia, Y. M.; Wu, H. P.; Zhang, Y.; Fang, Y.; Sun, S. Y.; Shi, Y. G. Synthesis and Application of Ionic Liquids in Enzymatic Catalysis. *Prog. Chem.* **2006**, *18* (12), 1660−1667.
(9) van Rantwijk, F.; Sheldon, R. A. Biocatalysis in Ionic Liquids. *Chem. Rev.* **2007**, *107* (6), 2757−2785.
(10) Moniruzzaman, M.; Nakashima, K.; Kamiya, N.; Goto, M. Recent Advances of Enzymatic Reactions in Ionic Liquids. *Biochem. Eng. J.* **2010**, *48* (3), 295−314.
(11) Moniruzzaman, M.; Kamiya, N.; Nakashima, K.; Goto, M. Water-in-Ionic Liquid Microemulsions as a New Medium for Enzymatic Reactions. *Green Chem.* **2008**, *10* (5), 497−500.
(12) Xue, L. Y.; Li, Y.; Zou, F. X.; Lu, L.; Zhao, Y.; Huang, X. R.; Qu, Y. B. The Catalytic Efficiency of Lipase in a Novel Water-in-[bmim][PF6] Microemulsion Stabilized by both AOT and Triton X-100. *Colloid Surf. B* **2012**, *92*, 360−366.
(13) Moniruzzaman, M.; Kamiya, N.; Goto, A. Biocatalysis in Water-in-Ionic Liquid Microemulsions: A Case Study with Horseradish Peroxidase. *Langmuir* **2009**, *25* (2), 977−982.
(14) Zhou, G. P.; Zhang, Y.; Huang, X. R.; Shi, C. H.; Liu, W. F.; Li, Y. Z.; Qu, Y. B.; Gao, P. J. Catalytic Activities of Fungal Oxidases in Hydrophobic Ionic Liquid 1-Butyl-3-Methylimidazolium Hexafluorophosphate-Based Microemulsion. *Colloid Surf. B* **2008**, *66* (1), 146−149.
(15) Xue, L. Y.; Qiu, H. J.; Li, Y.; Lu, L.; Huang, X. R.; Qu, Y. B.; Novel Water-in-Ionic, A. Liquid Microemulsion and its Interfacial Effect on the Activity of Laccase. *Colloid Surf. B* **2011**, *82* (2), 432−437.
(16) Zhao, H.; Campbell, S. M.; Jackson, L.; Song, Z. Y.; Olubajo, O. Hofmeister Series of Ionic Liquids: Kosmotropic Effect of Ionic Liquids on the Enzymatic Hydrolysis of Enantiomeric Phenylalanine Methyl Ester. *Tetrahedron: Asymmetry* **2006**, *17* (3), 377−383.
(17) Zhao, H.; Olubajo, O.; Song, Z. Y.; Sims, A. L.; Person, T. E.; Lawal, R. A.; Holley, L. A. Effect of Kosmotropicity of Ionic Liquids on the Enzyme Stability in Aqueous Solutions. *Bioorg. Chem.* **2006**, *34* (1), 15−25.
(18) Salvador, A. C.; Santos, M. D.; Saraiva, J. A. Effect of the Ionic Liquid [bmim]Cl and High Pressure on the Activity of Cellulase. *Green Chem.* **2010**, *12* (4), 632−635.
(19) Lu, L.; Hu, Y.; Huang, X. R.; Qu, Y. B.; Bioelectrochemical, A. Method for the Quantitative Description of the Hofmeister Effect of Ionic Liquids in Aqueous Solution. *J. Phys. Chem. B* **2012**, *116* (36), 11075−11080.
(20) Fujita, K.; MacFarlane, D. R.; Forsyth, M. Protein Solubilising and Stabilising Ionic Liquids. *Chem. Commun.* **2005**, *38*, 4804−4806.
(21) Fujita, K.; Forsyth, M.; MacFarlane, D. R.; Reid, R. W.; Eiliott, G. D. Unexpected Improvement in Stability and Utility of Cytochrome C by Solution in Biocompatible Ionic Liquids. *Biotechnol. Bioeng.* **2006**, *94* (6), 1209−1213.
(22) Fujita, K.; MacFarlane, D. R.; Forsyth, M.; Yoshizawa-Fujita, M.; Murata, K.; Nakamura, N.; Ohno, H. Solubility and Stability of Cytochrome C in Hydrated Ionic Liquids: Effect of Oxo Acid Residues and Kosmotropicity. *Biomacromolecules* **2007**, *8* (7), 2080−2086.
(23) Baker, G. A.; Heller, W. T. Small-Angle Neutron Scattering Studies of Model Protein Denaturation in Aqueous Solutions of the Ionic Liquid 1-Butyl-3-Methylimidazolium Chloride. *Chem. Eng. J.* **2009**, *147* (1), 6−12.
(24) Akdogan, Y.; Junk, M. J. N.; Hinderberger, D. Effect of Ionic Liquids on the Solution Structure of Human Serum Albumin. *Biomacromolecules* **2011**, *12* (4), 1072−1079.
(25) Sasmal, D. K.; Mondal, T.; Sen Mojumdar, S.; Choudhury, A.; Banerjee, R.; Bhattacharyya, K. An FCS Study of Unfolding and Refolding of CPM-Labeled Human Serum Albumin: Role of Ionic Liquid. *J. Phys. Chem. B* **2011**, *115* (44), 13075−13083.
(26) Chowdhury, R.; Mojumdar, S. S.; Chattoraj, S.; Bhattacharyya, K. Effect of Ionic Liquid on the Native and Denatured State of a Protein Covalently Attached to a Probe: Solvation Dynamics Study. *J. Chem. Phys.* **2012**, *137* (5), 055104−8.
(27) Singh, T.; Bharmoria, P.; Morikawa, M.; Kimizuka, N.; Kumar, A. Ionic Liquids Induced Structural Changes of Bovine Serum Albumin in Aqueous Media: A Detailed Physicochemical and Spectroscopic Study. *J. Phys. Chem. B* **2012**, *116* (39), 11924−11935.
(28) Wang, X.; Liu, J.; Sun, L.; Yu, L.; Jiao, J.; Wang, R. Interaction of Bovine Serum Albumin with Ester-Functionalized Anionic Surface-Active Ionic Liquids in Aqueous Solution: A Detailed Physicochemical and Conformational Study. *J. Phys. Chem. B* **2012**, *116* (41), 12479−12488.
(29) Heller, W. T.; O'Neill, H. M.; Zhang, Q.; Baker, G. A. Characterization of the Influence of the Ionic Liquid 1-Butyl-3-methylimidazolium Chloride on the Structure and Thermal Stability of Green Fluorescent Protein. *J. Phys. Chem. B* **2010**, *114* (43), 13866−13871.
(30) Heller, W. T. Small-Angle Neutron Scattering and Contrast Variation: A Powerful Combination for Studying Biological Structures. *Acta Crystallogr. Sect. D* **2010**, *66*, 1213−1217.
(31) Doniach, S. Changes in Biomolecular Conformation Seen by Small Angle X-ray Scattering. *Chem. Rev.* **2001**, *101* (6), 1763−1778.
(32) Koch, M. H. J.; Vachette, P.; Svergun, D. I. Small-Angle Scattering: A View on the Properties, Structures and Structural Changes of Biological Macromolecules in Solution. *Q. Rev. Biophys.* **2003**, *36* (2), 147−227.
(33) Svergun, D. I.; Koch, M. H. J. Small-Angle Scattering Studies of Biological Macromolecules in Solution. *Rep. Prog. Phys.* **2003**, *66* (10), 1735−1782.
(34) Zhao, J. K.; Gao, C. Y.; Liu, D. The Extended Q-Range Small-Angle Neutron Scattering Diffractometer at the SNS. *J. Appl. Crystallogr.* **2010**, *43*, 1068−1077.
(35) Glatter, O.; Kratky, O. *Small-angle X-ray Scattering*; Academic Press: London, 1982.
(36) Guinier, A.; Fournet, G. *Small-angle Scattering of X-rays*; Wiley: New York, 1955.
(37) Moore, P. B. Small-Angle Scattering - Information-Content and Error Analysis. *J. Appl. Crystallogr.* **1980**, *13* (APR), 168−175.
(38) Sugio, S.; Kashima, A.; Mochizuki, S.; Noda, M.; Kobayashi, K. Crystal Structure of Human Serum Albumin at 2.5 Angstrom Resolution. *Protein Eng.* **1999**, *12* (6), 439−446.
(39) Tjioe, E.; Heller, W. T. ORNL_SAS: Software for Calculation of Small-Angle Scattering Intensities of Proteins and Protein Complexes. *J. Appl. Crystallogr.* **2007**, *40*, 782−785.
(40) Kline, S. R. Reduction and Analysis of SANS and USANS Data using IGOR Pro. *J. Appl. Crystallogr.* **2006**, *39*, 895−900.
(41) Das, A.; Chitra, R.; Choudhury, R. R.; Ramanadham, M. Structural Changes During the Unfolding of Bovine Serum Albumin in the Presence of Urea: A Small-Angle Neutron Scattering Study. *Pramana* **2004**, *63* (2), 363−368.
(42) Lee, C. T.; Smith, K. A.; Hatton, T. A. Photocontrol of Protein Folding: The Interaction of Photosensitive Surfactants with Bovine Serum Albumin. *Biochemistry* **2005**, *44* (2), 524−536.
(43) Baker, S. N.; Zhao, H.; Pandey, S.; Heller, W. T.; Bright, F. V.; Baker, G. A. Fluorescence Energy Transfer Efficiency in Labeled Yeast Cytochrome C: A Rapid Screen for Ion Biocompatibility in Aqueous Ionic Liquids. *Phys. Chem. Chem. Phys.* **2011**, *13* (9), 3642−3644.